Battle, MW, Ewing, SF, Dickson, C, Obaje, J, Edgeworth, KN, Bindbeutel, R, Antoniou-Kourounioti, RL, Nusinow, DA and Jones, MA

Manipulation of photosensory and circadian signaling restricts phenotypic plasticity in response to changing environmental conditions in Arabidopsis

CellPress
Partner Journal

Molecular Plant
Research report

Manipulation of photosensory and circadian signaling restricts phenotypic plasticity in response to changing environmental conditions in *Arabidopsis*

Martin William Battle[1], Scott Fraser Ewing[1], Cathryn Dickson[1], Joseph Obaje[1,4], Kristen N. Edgeworth[2,3], Rebecca Bindbeutel[2], Rea L. Antoniou-Kourounioti[1], Dmitri A. Nusinow[2,*] and Matthew Alan Jones[1,*]

[1]Plant Science Group, School of Molecular Biosciences, University of Glasgow, Glasgow G12 8QQ, UK

[2]Danforth Plant Science Center, St. Louis, MO 63132, USA

[3]Department of Biological and Biomedical Sciences, Washington University in St. Louis, St. Louis, MO 63130, USA

[4]Present address: School of Biological and Environmental Sciences, Liverpool John Moores' University, Liverpool L2 2QP, UK

***Correspondence: Matthew Alan Jones (matt.jones@glasgow.ac.uk), Dmitri A. Nusinow (meter@danforthcenter.org)**

https://doi.org/10.1016/j.molp.2024.07.007

ABSTRACT

Plants exploit phenotypic plasticity to adapt their growth and development to prevailing environmental conditions. Interpretation of light and temperature signals is aided by the circadian system, which provides a temporal context. Phenotypic plasticity provides a selective and competitive advantage in nature but is obstructive during large-scale, intensive agricultural practices since economically important traits (including vegetative growth and flowering time) can vary widely depending on local environmental conditions. This prevents accurate prediction of harvesting times and produces a variable crop. In this study, we sought to restrict phenotypic plasticity and circadian regulation by manipulating signaling systems that govern plants' responses to environmental signals. Mathematical modeling of plant growth and development predicted reduced plant responses to changing environments when circadian and light signaling pathways were manipulated. We tested this prediction by utilizing a constitutively active allele of the plant photoreceptor phytochrome B, along with disruption of the circadian system via mutation of *EARLY FLOWERING3*. We found that these manipulations produced plants that are less responsive to light and temperature cues and thus fail to anticipate dawn. These engineered plants have uniform vegetative growth and flowering time, demonstrating how phenotypic plasticity can be limited while maintaining plant productivity. This has significant implications for future agriculture in both open fields and controlled environments.

Key words:: circadian, developmental plasticity, phenotypic plasticity, external coincidence, light, temperature

Battle M.W., Ewing S.F., Dickson C., Obaje J., Edgeworth K.N., Bindbeutel R., Antoniou-Kourounioti R.L., Nusinow D.A., and Jones M.A. (2024). Manipulation of photosensory and circadian signaling restricts phenotypic plasticity in response to changing environmental conditions in *Arabidopsis*. Mol. Plant. **17**, 1458–1471.

INTRODUCTION

Phenotypic plasticity enables plants to adapt to micro-niches within their environment but is problematic in modern agriculture, which benefits from uniform and predictable growth and reliable harvest times. In addition to experiencing daily and seasonal climatic differences, plants respond to light and temperature signals differentially, dependent upon time of day (Millar, 2016). Photo- and thermo-sensors work in combination with the circadian system, which provides an internal timing reference relative to dawn and dusk (Sanchez et al., 2020; Kerbler and Wigge, 2023). The plant circadian system continually integrates light and temperature as entrainment signals to modulate development, with a suite of photoreceptors, including phytochromes (phytochrome A [phyA] through phyE), cryptochromes (cryptochromes 1–3), zeitlupe (ZTL), and UVR8 each integrating light signals into the circadian clock (Somers

Published by the Molecular Plant Shanghai Editorial Office in association with Cell Press, an imprint of Elsevier Inc., on behalf of CSPB and CEMPS, CAS.

et al., 1998, 2004; Fehér et al., 2011; Webb et al., 2019; Sanchez et al., 2020). Phytochromes have been proposed to associate with promoters to alter gene expression, in part by specifying alternate promoter selection, although a role for phytochromes as transcriptional repressors has also been proposed (Chen et al., 2014; Jung et al., 2016; Ushijima et al., 2017; Balcerowicz et al., 2021). In line with this, phyB has been shown to interact with EARLY FLOWERING3 (ELF3), a chromatin-associated transcriptional repressor with a vital role in the circadian system (McWatters et al., 2000; Covington et al., 2001; Liu et al., 2001; Thines and Harmon, 2010; Huang et al., 2016a).

ELF3 was originally identified from a mutant screen to identify lines with accelerated flowering but was quickly noted to be essential for the maintenance of circadian rhythms in constant light (Hicks et al., 1996; Zagotta et al., 1996). Detailed studies suggest that the inhibition of circadian rhythms under constant illumination is caused by the loss of circadian gating of light signaling

(McWatters et al., 2000; Thines and Harmon, 2010). Later work described ELF3 as an integral part of the Evening Complex that enables interactions between ELF4 and LUX ARRHYTHMO and represses gene expression during the night (Nusinow et al., 2011). Higher-order mutant analyses and genome-wide studies demonstrate that phyB and ELF3 have additive roles in regulating hypocotyl length and flowering time (Reed et al., 2000; Ezer et al., 2017), while *phyb* exacerbates the shortened circadian free-running period of *elf3-12* seedlings (Kolmos et al., 2011). Interestingly, ELF3 and phyB have both been shown to be responsive to temperature as well as contributing to circadian timing and photoperception (Jung et al., 2016, 2020; Legris et al., 2016).

Although phyB and ELF3 bind one another, we still do not understand how ELF3 and phyB interact to maintain circadian rhythms and regulate plant development (Liu et al., 2001; Huang et al., 2016a). Here, we revised mathematical models of the circadian system to better interpret phyB and ELF3 interactions and utilized a constitutively active allele of phyB (Y276→H [YHB]) in combination with a null *ELF3* allele to examine whether these crucial components of the plant sensory system can be engineered to limit responses to environmental cues.

RESULTS AND DISCUSSION

Modeling refines our understanding of light input into the circadian system

Decades of research suggest that the phyB and ELF3 signaling pathways are genetically separable, although multiple lines of evidence demonstrate a functional interaction between these signaling pathways (Reed et al., 2000; Covington et al., 2001; Liu et al., 2001; Yu et al., 2008; Kolmos et al., 2011; Jung et al., 2016; Legris et al., 2016; Nieto et al., 2022). Mathematical modeling of these interactions highlights the central contributions of phyB and ELF3 toward key aspects of development, such as seedling establishment and flowering time (Seaton et al., 2015; Chew et al., 2022). Disruption of ELF3 function induces consistently early flowering but imposes an etiolated phenotype that is reproduced by the *Arabidopsis* Framework Model (FMv2; Supplemental Figure 1A–1C) (Seaton et al., 2015; Chew et al., 2022). Since increased phyB activity (either through overexpression or inclusion of a constitutively active YHB allele) promotes photomorphogenesis via post-translational regulation of PHYTOCHROME INTERACTING FACTORs (PIFs), we expected that YHB would be epistatic to *elf3* with regards photomorphogenesis (Wagner et al., 1991; Su and Lagarias, 2007; Hajdu et al., 2015). FMv2 aligned with our hypothesis that increased phyB signaling in the absence of ELF3 (modeled by increasing light inputs into the P2012 circadian module and S2015 photoperiodism module) would limit hypocotyl growth while retaining an early-flowering phenotype (Supplemental Figure 1A–1C).

Plants expressing *YHB* maintain robust circadian rhythms in constant darkness compared to the wild type, although it remains unclear how phyB-initiated signals are integrated into the circadian system (Jones et al., 2015; Huang et al., 2019). We examined two alternate hypotheses to apply constitutive phyB signaling into the circadian module of FMv2 (Supplemental Figure 1D). Initially, we investigated whether constitutive phyB signaling acted by promoting light-induced gene expression within the model as well as repressing COP1 accumulation (Supplemental Figure 1D). This "global phyB effect" could not reconstitute YHB-mediated circadian rhythms in FMv2 after transfer to constant darkness (Supplemental Figure 1E). Interestingly, work examining dawn-induced gene expression suggests that photoreceptor activation is insufficient to promote transcript accumulation (Balcerowicz et al., 2021). Removing light-activated gene expression from our YHB simulation provided a "COP1 only" variant (Supplemental Figure 1D and 1F). The FMv2+COP1 variant retained circadian rhythms in constant darkness but was inconsistent with previous experimental data, since circadian behavior was similar to the wild type, and the early flowering phenotype of *YHB* plants was not predicted (Supplemental Figure 1D and 1F) (Pokhilko et al., 2012; Fogelmark and Troein, 2014; Hajdu et al., 2015; Jones et al., 2015; Huang et al., 2019).

This inconsistency within the model when compared to experimental data encouraged us to examine alternate circadian models. The F2014 circadian model revises the FMv2 circadian module to include refined waves of transcriptional repression based on experimental data (Fogelmark and Troein, 2014). The resultant "FMv2+F2014" model recapitulated YHB-mediated retention of circadian amplitude compared to damping in the wild type, although the model was unable to recapitulate the extension of the circadian period observed in YHB lines in constant darkness (Figure 1; Huang et al., 2019; Jones et al., 2015). The effect of YHB was apparent in both "global" and "COP1 only" approximations of YHB, although, again, the "COP1 only" variant matched the experimental luciferase data more closely (Figure 1B–1D) (Jones et al., 2015; Huang et al., 2019). Future model iterations incorporating transcriptional regulation from photosynthetically derived signals could further improve model predictions, particularly with regard to phase and period length (Queiroz et al., 2023). We next examined how disruption of *ELF3* was predicted to affect constitutive phyB signaling. Both FMv2 and FMv2+F2014

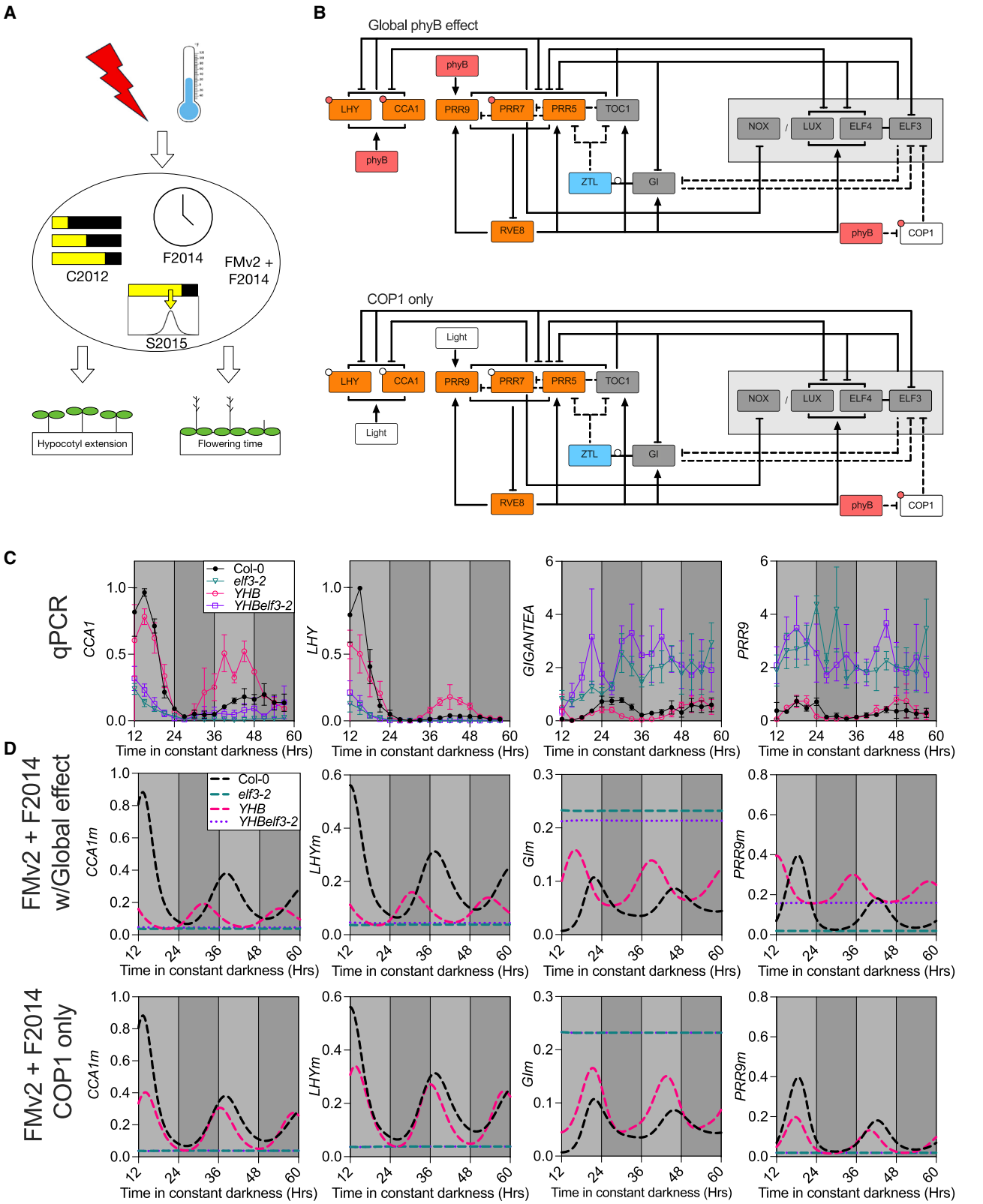

Figure 1. Modeling suggests that COP1-mediated activity is sufficient to integrate phyB signaling into the circadian system.
(A) Cartoon of FMv2 including the F2014 circadian model (FMv2+F2014). C2012 and S2015 are distinct modules that model phenology and photoperiodism, respectively (Chew et al., 2022).

(legend continued on next page)

models predict that *elf3* will be epistatic to *YHB* regarding circadian rhythmicity (Figure 1 and Supplemental Figure 1) (McWatters et al., 2000; Covington et al., 2001; Thines and Harmon, 2010; Huang et al., 2016a).

The combination of *YHB* and *elf3* alleles restricts daily patterns of gene expression

We next sought to reproduce these predictions *in planta* by introducing the *YHB* allele into *elf3* (Su and Lagarias, 2007; Hu et al., 2009; Nusinow et al., 2011). This allowed us to assess whether *YHBelf3* seedlings had phenotypes aligned with our modeled predictions, with the ultimate goal of minimizing phenotypic plasticity and circadian regulation in plants (Figure 2). *In vivo*, neither constitutive expression of *YHB* (*35S::YHB* [*elf3-1 phyb-9*]) nor expression of *YHB* driven by the endogenous *PHYB* promoter (*PHYB::YHB* [*elf3-2*]; *YHBelf3-2*) was able to maintain circadian rhythms of *CCA1*-driven bioluminescence in constant darkness, with only 15% of *YHBelf3-2* lines being assessed as rhythmic (Figure 2A and 2B and Supplemental Figure 2A and 2B) (Jones et al., 2015; Huang et al., 2019). RT–qPCR analysis of candidate genes (including *CCA1*, *LHY*, *GIGANTEA*, and *PSEUDORESPONSE REGULATOR9* [*PRR9*]) confirmed the loss of circadian rhythmicity in *YHBelf3-2* lines compared to *YHB* (Figure 1C). Interestingly, mis-regulation of these candidate circadian transcripts fell into two groups: *CCA1/LHY* (whose promoters are solely bound by phyB; Supplemental Figure 3) (Jung et al., 2016; Ezer et al., 2017) and *GI/PRR9* (bound by both phyB and ELF3; Supplemental Figure 3) (Jung et al., 2016; Ezer et al., 2017). For each transcript, accumulation patterns over time were consistent in *elf3-2* and *YHBelf3-2* seedlings (Figure 1C). Although the FMv2+F2014 model aligned with experimental transcript accumulation for *CCA1*, *LHY*, and *GIGANTEA*, we were interested to note that the FMv2+F2014 model predicted *PRR9* mRNA to damp to basal levels in *elf3* and *YHBelf3* plants (Figure 1D). This contrasts our experimental data which demonstrates elevated (and arrhythmic) *PRR9* accumulation in *elf3-2* and *YHBelf3-2* plants (Figure 1D). Such data indicate that ELF3 is necessary to retain circadian rhythms but highlight the limitations of existing mathematical models to fully reconstitute the circadian system.

ELF3 and YHB signaling programs interact to affect the expression of photomorphogenic and circadian genes

To further explore the regulation of gene expression in *YHBelf3-2* seedlings, we used RNA sequencing (RNA-seq) to assess transcript accumulation in plants 48 h after transfer to constant darkness at dusk (Zeitgeber Time [ZT] 60), a time point at which wild-type seedlings appeared to have become arrhythmic and therefore had relatively stable levels of circadian-controlled transcript abundance (Figure 1C, 2A and Supplemental Figure 4). Although starvation markers were upregulated in all genotypes (e.g., ATL8 and KMD4; Graf et al., 2010), circadian rhythms persisted in *YHB* seedlings at ZT60, suggesting that circadian rhythms are actively damped in a phyB-dependent manner (Jones et al., 2015; Huang et al., 2019).

We first determined log fold change (-log2FC) in *elf3-2*, *YHB*, and *YHBelf3-2* genotypes relative to the wild type (Supplemental Figure 4; Supplemental Table 1). As expected, Gene Ontology (GO) terms associated with responses to light stimuli were over-represented in our lists of genes mis-expressed in *YHB* and *YHBelf3-2* (Supplemental Figure 5; Supplemental Table 2). GO terms associated with circadian rhythms were also significantly over-represented (Supplemental Figure 5; Supplemental Table 2). We next examined whether mis-regulated transcripts in each genotype tended to be expressed at particular times of day by assessing whether mis-expressed genes were over- or under-represented at different times (Figure 2C) (Bonnot et al., 2022). Significantly mis-accumulated transcripts were not confined to a single time period in *elf3-2*, *YHB*, or *YHBelf3-2* lines, suggesting that the circadian system is not "locked" at a particular circadian phase in any of these genotypes (Figure 2C). Instead, differences in the accumulation of numerous core circadian transcripts were apparent (Supplemental Figure 4A–4D) (Hsu and Harmer, 2014; Laosuntisuk et al., 2023). In constant darkness, *elf3-2* plants accumulate increased levels of *GIGANTEA*, *PRR9*, and *BROTHER OF LUX ARRHYTHMO*, whereas *CCA1*, *LHY*, and *REVEILLE8* steady-state levels are reduced (Supplemental Figure 4A). Ten of the notional 60 core clock genes are highly mis-accumulated in *YHB* relative to the wild type (9 upregulated and 1 downregulated; Supplemental Figure 4A and 4C).

To further address how YHB and ELF3 govern photomorphogenesis, we examined differential expression of genes associated with a response to light stimuli using our RNA-seq dataset of dark-adapted plants (Supplemental Figure 4E–4H) (GO:0009416) (Ashburner et al., 2000; Gene Ontology Consortium, 2023). Of the 740 light stimulus-associated transcripts examined, only 33 are mis-regulated in *elf3-2* plants, with 6 downregulated and 27 upregulated transcripts (Supplemental Table 1). Of these, *elf3-2* and *YHBelf3-2* plants share only 7 mis-regulated transcripts, one of which (*HOMEOBOX-LEUCINE ZIPPER PROTEIN 4* [*HB4*]) has been shown previously to play a role in shade avoidance via both phytochrome signaling and ELF3 (Supplemental Figure 4E–4H) (Sorin et al., 2009; Jiang et al., 2019). *HB4* is downregulated in *elf3-2* but upregulated in *YHB* and *YHBelf3-2* (Supplemental Figure 4E–4H; Supplemental Table 1). By contrast, 113

(B) PhyB signaling into the circadian system was modeled via two hypotheses. The "global phyB effect" variant (top) proposes that activated phyB is sufficient to induce light-activated gene expression in the circadian system in addition to enabling degradation of COP1. The "COP1 only" variant (bottom) restricts the effect of phyB activation solely to the turnover of COP1. In both cases, stability of ZTL and GI is regulated independently, since this is a blue light-mediated effect (Kim et al., 2013). The Circadian model adapted from F2014 (Fogelmark and Troein, 2014). Post-translational regulation by light is indicated by small white circles. Small red circles indicate post-translational regulation induced by phyB.
(C) Accumulation of *CCA1*, *LHY*, *GIGANTEA*, and *PRR9* in constant darkness. Plants were entrained in 12:12 light:dark cycles for 12 days before being transferred to constant darkness at dusk (ZT12). Tissue was sampled every 3 h at the indicated time points. Data presented are the average of three independent biological replicates and are presented relative to accumulation of *APA1*, *APX3*, and *IPP2* transcripts. Error bars indicate SEM.
(D) Modeled accumulation of *CCA1m* (*CCA1* mRNA), *LHYm* (*LHY* mRNA), *GIm* (*GIGANTEA* mRNA), and *PRR9m* (*PRR9* mRNA) in constant darkness. Light gray bars demonstrate subjective day in constant darkness.

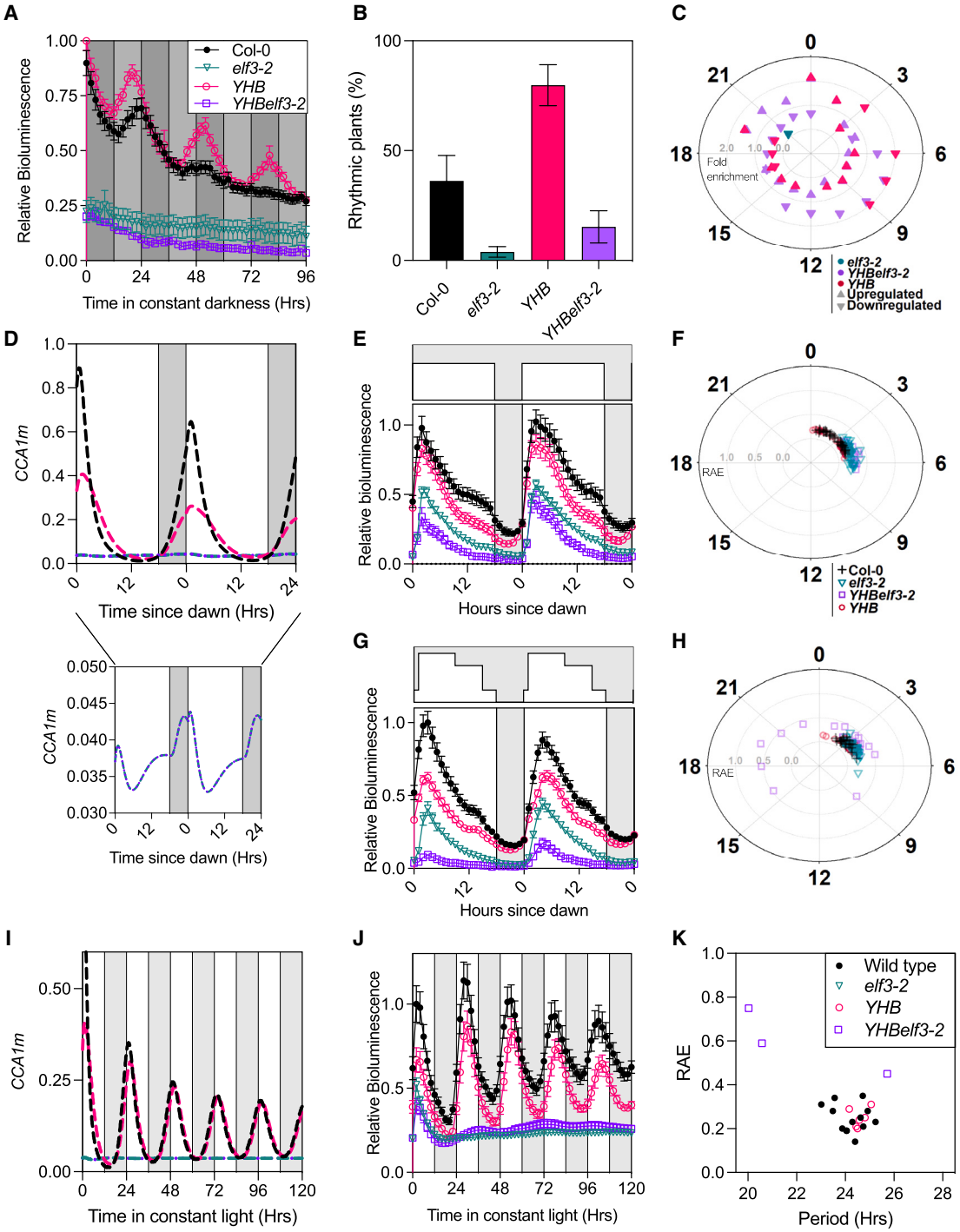

Figure 2. *YHBelf3-2* plants lack circadian rhythms but retain modest responses to light cues.

(A) Waveforms of luciferase bioluminescence rhythms of wild-type (Col-0, black), *YHB* (pink), *elf3-2* (green), and *YHBelf3-2* (purple) seedlings expressing a *CCA1::LUC2* reporter, entrained for 7 days under 12 h:12 h light:dark cycles (indicated before time point 0 by white and gray bars, respectively) before transfer to constant darkness (with subjective day:night cycles in constant darkness indicated by gray and light gray bars after time point 0).

(B) Percentage of seedlings measured in **(A)**, which presented robust circadian rhythms (calculated using BioDare; www.biodare2.ed.ac.uk; Zielinski et al., 2014). Data are presented as mean ± SEM from three independent experiments.

(C) Plot showing phase distribution of mis-accumulated transcripts (log2FC > 1.0 or < −1.0 and $p < 0.05$) in each genotype relative to the wild type separated by phase using CAST-R (Bonnot et al., 2022). The y axis depicts fold enrichment compared to the reference dataset. Statistical significance was determined using a chi-square test (Bonnot et al., 2022). Plants were harvested 48 h after transfer to constant darkness (ZT60). Pyramids indicate up-regulated genes, and inverted pyramids represent down-regulated genes; colors as in **(A)**.

(D) Modeled accumulation of *CCA1m* (*CCA1* mRNA) in 12:12 light:dark cycles. Dark gray bars indicate periods of darkness.

(legend continued on next page)

transcripts are significantly differentially expressed in *YHB* plants relative to the wild type, with 83 being upregulated and 30 downregulated (Supplemental Figure 4G–4H; Supplemental Table 1). Ninety-one of these transcripts are similarly differentially expressed in both *YHB* and *YHBelf3-2* plants (Supplemental Figure 4G–4H).

We further dissected interactions between *YHB*- and *elf3*-affected transcript accumulation by assessing differential gene expression in *YHBelf3-2* seedlings compared to either *YHB* or *elf3-2* (Supplemental Figure 4I–4M). There was little correlation in expression levels between genes differentially expressed in *elf3-2* relative to Col-0 and *YHBelf3-2* relative to *YHB*, suggesting that the loss of ELF3 has different effects upon global transcript accumulation in the presence or absence of YHB (Supplemental Figure 4I; $R < 0.35$). However, we observed a strong correlation in differential gene expression when comparing transcripts misexpressed in *YHB* relative to Col-0 and *YHBelf3-2* relative to *elf3-2* (Supplemental Figure 4J; $R > 0.8$). This correlation was retained when we divided our data into circadian-regulated and circadian-independent transcripts and when we assessed the accumulation of light-responsive transcripts (Supplemental Figure 4J and 4L). These data suggest an epistatic effect of constitutive phyB signaling upon photomorphogenesis despite the inter-related nature of phyB- and ELF3-mediated effects upon gene expression (Nieto et al., 2022).

By comparison, ELF3 had a stronger role in regulating core circadian transcripts (Supplemental Figure 4M and 4N). *YHB* expression continued to affect the accumulation of some core circadian transcripts in the absence of ELF3, but the majority of differentially expressed core clock transcripts were well correlated (when comparing *elf3-2* relative to Col-0 and *YHBelf3-2* relative to *YHB*; Supplemental Figure 4M, $R = 0.8$). Equally, the misexpression of numerous core circadian transcripts was altered when comparing *YHB* relative to Col-0 and *YHBelf3-2* relative to *elf3-2* (Supplemental Figure 4N). These data align with the essential role of *ELF3* within the circadian system (Covington et al., 2001; Thines and Harmon, 2010) while highlighting putative loci where YHB affects core clock transcript accumulation separately from ELF3.

YHBelf3 plants have a reduced response to light:dark cycles

We next examined the behavior of *YHBelf3* seedlings in the presence of light. Although our modeling expected that *elf3* and *YHBelf3* would essentially be arrhythmic in response to dawn and dusk (Figure 2D), each of the genotypes examined displayed circadian entrainment to experimental light signals and retained daily responses to dawn, as depicted by the calculated phase of *CCA1::LUC2* bioluminescence in driven light:dark cycles (Figure 2E and 2F). *CCA1::LUC2* bioluminescence began to increase in wild-type and *YHB* seedlings 1–3 h before dawn, indicating a circadian anticipation of dawn in these plants (Figure 2E). By contrast, this dawn anticipation was absent in *elf3-2* and *YHBelf3-2* plants, with *CCA1::LUC2*-driven bioluminescence increasing only after the application of light (Figure 2E). These data suggest that *elf3-2* and *YHBelf3-2* retain photosensitivity despite the disruption of circadian rhythmicity in these lines.

Since *elf3-2* and *YHBelf3-2* plants retained a response to dawn, we examined the activation of the *CCA1* promoter in response to varied light intensity during the photoperiod (Figure 2G and 2H). A pseudo-sinusoidal regime was designed, where light intensity varied throughout the day, peaking in the late morning and gradually decreasing as dusk approached (Figure 2G). Our experimental data demonstrated that *elf3-2* retained entrainment to pseudo-sinusoidal lighting, although *YHBelf3-2* was less able to entrain to these conditions (Figure 2G and 2H). These data are consistent with additional photosensory systems feeding into the regulation of *CCA1*, including metabolic signals from photosynthesis (Haydon et al., 2013; Jones, 2018, 2019; Wang et al., 2024).

We next assessed circadian rhythmicity in *YHBelf3* seedlings held in constant light. Our modeling predicted that wild-type and *YHB* seedlings would have comparable circadian rhythms in constant light (Figure 2I). In line with this hypothesis, circadian rhythms in *YHB* seedlings were indistinguishable from the wild type in constant white light, although the phase of *CCA1::LUC+* activity was approximately 6 h later than modeled *CCA1* mRNA (Figure 2I–2K). This delay in phase may reflect time required for luciferase translation or could indicate that light inputs into the F2014 model require further refinement to include photosynthetic signals or additional photoreceptor control. Despite these caveats, the model was able to reproduce the dissipation of circadian rhythms in *elf3-2* and *YHBelf3-2* seedlings within 24 h of transfer to constant white light (Figure 2J–2K).

YHBelf3-2 plants have reduced growth and flowering plasticity in response to light and temperature cues

The combination of *YHB* and *elf3* alleles decouples the circadian system from photomorphogenesis, although *YHBelf3-2* plants can retain daily patterns of gene expression when

(E) Patterns of luciferase bioluminescence rhythms of Col-0, *YHB*, *YHBelf3-2*, and *elf3-2* seedlings expressing a *CCA1::LUC2* reporter in 12:12 light:dark cycles.
(F) Phase distribution plot showing time of peak *CCA1*-driven luciferase bioluminescence calculated from **(D)**. The y axis depicts relative amplitude error (RAE).
(G) Patterns of luciferase bioluminescence rhythms of Col-0, *YHB*, *YHBelf3-2*, and *elf3-2* seedlings expressing a *CCA1::LUC2* reporter, entrained for 7 days in pseudo-sinusoidal light conditions (cycles of 1 h 10 μmol m^{-2} s^{-1}, 8 h 40 μmol m^{-2} s^{-1}, 6 h 30 μmol m^{-2} s^{-1}, and 3 h 10 μmol m^{-2} s^{-1} white light, followed by 6 h of darkness).
(H) Phase distribution plot showing time of peak *CCA1*-driven luciferase bioluminescence calculated from **(G)**. The y axis depicts RAE.
(I) Modeled accumulation of *CCA1m* (*CCA1* mRNA) in constant light. Light gray bars indicate periods of subjective darkness.
(J) Waveforms of luciferase bioluminescence rhythms of wild-type (Col-0), *elf3-2*, *YHB*, and *YHBelf3-2* seedlings expressing a *CCA1::LUC2* reporter, entrained for 7 days under 12 h:12 h light:dark cycles and constant 22°C temperature before transfer to constant light for imaging.
(K) Assessment of rhythmic robustness (RAE) plotted against circadian free-running period for data presented in **(J)**. Experimental data are representative of 3 independent experiments ($n \geq 15$). Error bars indicate SEM.

grown in light:dark cycles (Figure 1 and 2). We were therefore interested how our genetic manipulations affected developmental traits and life cycle transitions in varied light conditions (Figure 3). Our FMv2+F2014 model predicted that hypocotyl length would be uncoupled from photoperiod in *YHBelf3* (Figure 3A). We observed that *YHB*-driven growth phenotypes persisted in the hypocotyls of 5-day old seedlings (Figure 3B and 3D). *YHBelf3-2* seedlings retained a short hypocotyl phenotype regardless of the light condition utilized for growth and with no significant difference observed between *YHB* and *YHBelf3-2* seedlings (Figure 3B–3D). We note that *YHB* and *YHBelf3-2* seedlings were indistinguishable from the wild type when grown under long-day conditions (Figure 3D). Ranking of phenotypic plasticity between genotypes highlighted that the hypocotyl length of *elf3-2* seedlings was more sensitive to the photoperiod than the wild type, whereas *YHB* and *YHBelf3-2* seedlings were less responsive (Supplemental Table 4) (Arnold et al., 2019).

We next examined growth phenotypes in more mature *Arabidopsis* plants (3 weeks after sowing; Figure 3E and 3F and Supplemental Figure 6). The size of wild-type *Arabidopsis* plants is greatly dependent upon photoperiod length when plants are grown at 22°C, with the rosette diameter decreasing as the photoperiod increases (Figure 3E and 3F). *elf3-2* seedlings had an expanded rosette diameter compared to wild-type plants grown under long days, possibly related to the loss of light perception in these lines (Figure 3E and 3F) (Zagotta et al., 1996). We noted substantial variation in rosette diameter in wild-type and *elf3-2* plants, although rosette diameter was more consistent under longer photoperiods (Figure 3E and 3F). By contrast, the rosettes of *YHB* and *YHBelf3-2* seedlings were indistinguishable from each other, being more compact and uniform in size regardless of day length (Figure 3E and 3F).

The *YHB* and *elf3-2* genotypes have both been shown previously to have an early flowering phenotype when grown under short-day conditions, and so we expected that *YHBelf3-2* plants would share this phenotype (Figure 3G and 3H) (Zagotta et al., 1996; Franklin and Quail, 2010; Hajdu et al., 2015). Our FMv2+F2014 model similarly predicts that *YHBelf3* plants will display reduced photoperiodic sensitivity comparable to *elf3* (Figure 3G). In agreement with this hypothesis, *YHB*, *elf3*, and *YHBelf3-2* plants flowered earlier than the wild type under either long-day or short-day conditions (Figure 3G and 3H).

Both phyB and ELF3 are critical for temperature responses in addition to their roles in photoperception (Jung et al., 2016, 2020; Legris et al., 2016). We therefore compared how our *YHBelf3-2* plants performed under varying temperature conditions (Figure 4). In contrast to light-driven entrainment (Figs. 2E-F), *CCA1*-driven bioluminescence peaked 6 h after dawn in the wild type when entrained to temperature (Figure 4A and 4B). The phase of *CCA1*-driven bioluminescence was unaffected in *YHB* seedlings, although neither *elf3-2* nor *YHBelf3-2* seedlings could entrain to temperature signals when held in constant light (Figure 4A and 4B). These data suggest that light cues are necessary to drive rhythmic *CCA1* expression in *elf3* and *YHBelf3-2* seedlings.

As under different lighting regimes, *elf3-2* hypocotyls displayed greater plasticity than the wild type, with *YHB* and *YHBelf3-2* hypocotyls being less responsive to temperature than the wild type (Figure 4C; Supplemental Table 4) (Arnold et al., 2019). Seedling growth is therefore more uniform in *YHBelf3-2* plants compared to the wild type regardless of light or temperature cues, as reported previously for *YHB* alone (Jung et al., 2016). Ambient temperature also affected rosette diameter (Figure 4D and Supplemental Figure 6). Wild-type plants maintain a comparatively consistent diameter between 12°C and 27°C when grown in neutral day conditions (12:12 light:dark cycles), with a modest but significant decrease at 12°C (Figure 4D and Supplemental Figure 6; Supplemental Table 4). By contrast, *elf3-2* seedlings were more sensitive to lower temperatures, with rosette diameter substantially decreasing at 12°C and 17°C compared to higher temperatures (Figure 4D; Supplemental Table 4). *YHB* and *YHBelf3-2* plants were also responsive to these temperature changes, although the difference in size was smaller than that observed in *elf3-2* plants (Figure 4D; Supplemental Table 4). Under neutral day conditions, flowering was delayed in all genotypes when plants were grown at 12°C, but we were interested to note that *YHBelf3-2* plants flowered earlier than *YHB*, in contrast to other developmental phenotypes, where *YHB* effects were epistatic (Figure 4E; Supplemental Table 4). Flowering time accelerated in wild-type plants as temperatures increased (Figure 4E; Supplemental Table 4). By contrast, *YHB*, *elf3-2*, and *YHBelf3-2* genotypes retained stable flowering times from 17°C to 27°C (Figure 4E). The *YHB* and *YHBelf3-2* plants therefore retain uniform and early flowering phenotypes and so demonstrate reduced phenotypic plasticity across a range of light conditions and temperatures.

Photo- and thermo-morphogenesis are crucial processes that enable plants to optimize growth and development in response to prevailing environmental conditions by phenotypic plasticity. Our data validate mathematical models and demonstrate that expression of *YHB* is epistatic to the morphological consequences of *ELF3* disruption, although *ELF3* is essential to maintain circadian rhythmicity (Figures 1–3). *YHBelf3-2* plants consequently retain a vegetative phenotype comparable to the wild type but have an early flowering phenotype and cannot anticipate daily environmental transitions (Figure 3 and 4). The combination of *YHB* and *elf3* alleles consequently produces plants less responsive to environmental signals that retain vegetative growth and predictable flowering. This demonstrates how engineering the circadian system alongside environmental signaling pathways creates plants with more uniform growth and consistent environmental responses.

Although phenotypic plasticity is advantageous in natural conditions (where competition for resources and environmental stresses vary across seasons and locations), this trait is disadvantageous in modern crop monoculture where fertilizers, pesticides, irrigation, etc., can be provided. Reducing phenotypic plasticity and circadian regulation has potential beneficial implications for farming, and one goal of modern breeding programs has been to increase the uniformity of crops so that harvesting time is more predictable and quality is consistent. This applies to intensive, precision outdoor farming and total controlled environment agriculture (or vertical farming). In addition, climate change has rapidly altered day length and temperature relationships worldwide, and maintaining crop productivity in current locations or moving to more favorable temperate latitudes will

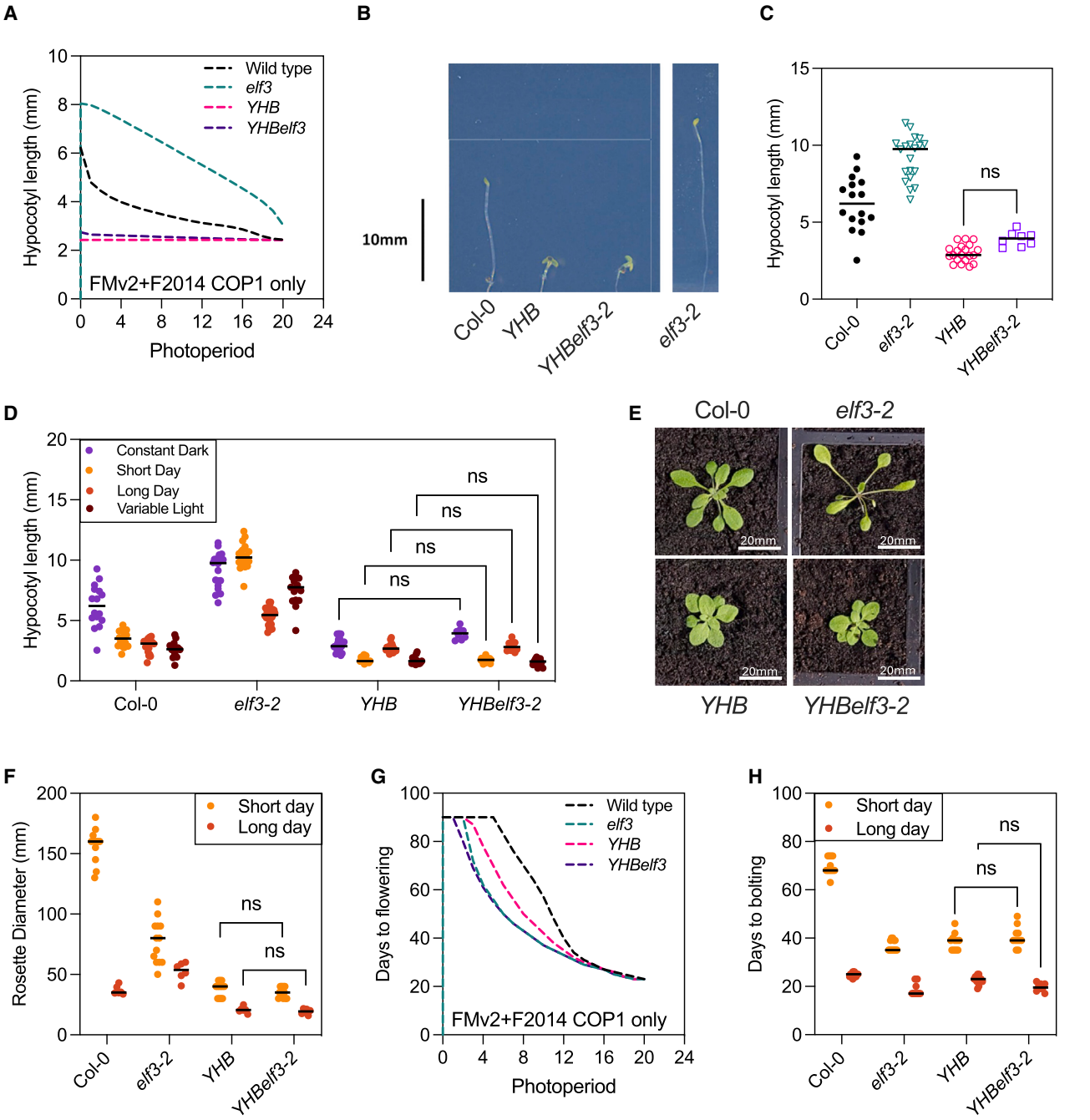

Figure 3. *YHBelf3* plants are less responsive to changing light environments.

(A) Modeled hypocotyl length in wild-type, *elf3*, *YHB*, and *YHBelf3* seedlings under different simulated photoperiods.

(B) Representative images of wild-type (Col-0), *YHB*, *YHBelf3-2* and *elf3-2* seedlings grown vertically on 0.5 MS plates for 5 days in constant darkness.

(C) Quantification of the hypocotyl lengths of Col-0, *YHB*, *YHBelf3-2*, and *elf3-2* seedlings grown vertically on 0.5 MS plates for 5 days in constant darkness. Data shows a representative example from 3 independent experiments ($n \geq 9$).

(D) Hypocotyl length of Col-0, *elf3-2*, *YHB*, and *YHBelf3-2* seedlings grown vertically on 0.5 MS plates for 5 days in constant darkness (purple), short day cycles (yellow), long day cycles (orange) or pseudo-sinusoidal light cycles (brown; cycles of 1 h 10 μmol m^{-2} s^{-1}, 8 h 40 μmol m^{-2} s^{-1}, 6 h 30 μmol m^{-2} s^{-1}, and 3 h 10 μmol m^{-2} s^{-1} white light, followed by 6 h of darkness).

(E) Representative images of Col-0, *YHB*, *YHBelf3-2*, and *elf3-2* seedlings grown on soil for 21 days under long day cycles (18 h:16 h light:dark) with 150 μmol m^{-2} s^{-1} white light and a constant temperature of 22°C.

(F) Rosette diameter of 28-day-old Col-0, *elf3-2*, *YHB*, and *YHBelf3-2* seedlings grown on soil under short or long days at 22°C.

(G) Modeled flowering time in wild-type, *elf3*, *YHB*, and *YHBelf3* seedlings under different simulated photoperiods.

(H) Flowering time of Col-0, *YHB*, *YHBelf3-2*, and *elf3-2* plants grown on soil at a constant temperature of 22°C under long or short days. Data show a representative example from 3 independent experiments ($n \geq 10$). Selected comparisons are presented from a two-way ANOVA, adjusted using Tukey's multiple-comparisons test.

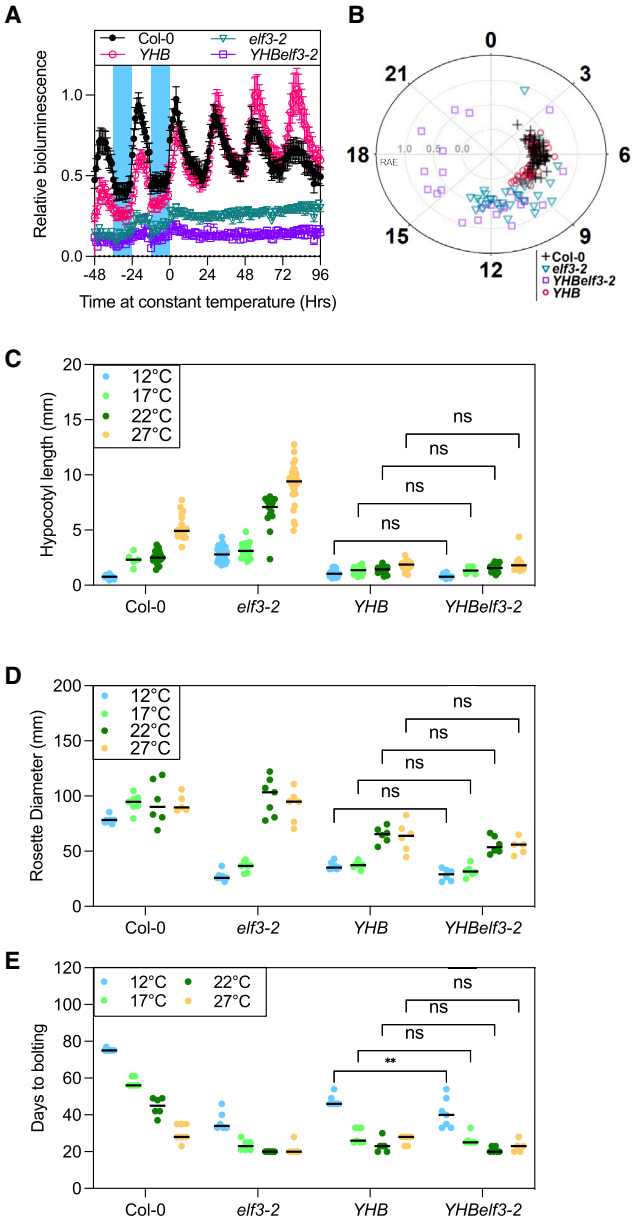

Figure 4. *YHBelf3* plants are less responsive to temperature-driven environmental cues.

(A) Patterns of luciferase bioluminescence rhythms of wild-type (Col-0), *elf3-2*, *YHB*, and *YHBelf3-2* seedlings expressing a *CCA1::LUC2* reporter, entrained for 7 days under 12 h:12 h 22°C:17°C cycles and constant white light before transfer to testing conditions at a constant temperature of 22°C.

(B) Phase distribution plot showing time of peak *CCA1*-driven luciferase bioluminescence calculated from **(A)**. Data are presented as the mean ± SEM and are representative of at least 3 independent experiments ($n \geq 15$). The y axis depicts RAE.

(C) Hypocotyl length of Col-0, *elf3-2*, *YHB*, and *YHBelf3-2* seedlings grown vertically on 0.5 MS plates for 5 days under 12 h:12 h light:dark cycles at a constant temperature of (from left to right) 12°C (blue), 17°C (light green), 22°C (dark green), or 27°C (yellow).

(D) Rosette diameter of 28-day-old Col-0, *elf3-2*, *YHB*, and *YHBelf3-2* seedlings grown on soil under 12 h:12 h light:dark cycles at a constant temperature of (from left to right) 12°C (blue), 17°C (light green), 22°C (dark green), or 27°C (yellow).

(E) Flowering time of Col-0, *elf3-2*, *YHB*, and *YHBelf3-2* plants grown on soil under 12 h:12 h light:dark cycles at a constant temperature of (from left to right) 12°C (blue), 17°C (light green), 22°C (dark green), or 27°C (yellow). Data are representative of at least three biological repeats. Error bars indicate SEM. Selected comparisons are presented from a two-way ANOVA, adjusted using Tukey's multiple-comparisons test.

require manipulation of environmental responses. Our modeling predicted that manipulating phyB and ELF3 signaling cascades would restrict phenotypic plasticity and circadian regulation in response to changing photoperiods (Figures 1–3). Crucially, we have shown that combining these two alleles (*YHBelf3*) limits phenotypic plasticity and circadian regulation while retaining earlier flowering times and maintaining vegetative growth (Figures 3 and 4). Since ELF3 and YHB have conserved function across species, it will be of great interest to apply these genetic modifications to reduce developmental variation in crops (Huang et al., 2017; Hu et al., 2020).

METHODS

Plant material and growth conditions

Wild-type *CCA1::LUC+* and *elf3-2 CCA1::LUC+ Arabidopsis* seeds have been reported previously (Huang et al., 2016a). *PHYB::YHB* and *PHYB::YHB* (*elf3-2*) *Arabidopsis* were generated by transforming *CCA1::LUC+* and *elf3-2 CCA1::LUC+* seeds with pJM63 gYHB (Su and Lagarias, 2007) via floral dip (Clough and Bent, 1998). Transformants were selected with 75 mg ml^{-1} kanamycin to identify homozygous seedlings in the T3 generation. *phyb-9 elf3-1* lines were generated by crossing *elf3-1* to CCA1::LUC+, and *phyB-9* was crossed to CCA1::LUC+, with long-hypocotyl, bioluminescent F2 seedlings confirmed for homozygous *elf3-1* and *phyB-9* alleles using a derived Cleaved Amplified Polymorphic Sequences (dCAPS) primer strategy as described previously (Nusinow et al., 2011; Huang et al., 2016b). *elf3-1* CCA1::LUC+ was then crossed to *elf3-1 phyB-9* (Reed et al., 2000), and bioluminescent, long-hypocotyl F2 lines were confirmed as *elf3-1 phyB-9* using the PCR strategy described above. F3 lines were screened for bioluminescence to identify homozygous CCA1::LUC+ seedlings.

The cerulean fluorescent protein (CER) was cloned from plasmid CER C1 (Koushik et al., 2006) using primers pDAN0869 and pDAN0870 and recombined with pB7-SHHc (Huang et al., 2016b) digested with AvrII using In-Fusion HD cloning (Clontech, Mountain View, CA, USA) to generate pB7-CER-SHHc. pENTR-YHB (Huang et al., 2016b) was recombined with pB7-CER-SHHc to generate pB7-YHB-CER-SHHc. This plasmid was transformed into *elf3-1 phyb-9 CCA1::LUC+* to generate *35S::PHYB(elf3-1 phyb-9) CCA1::LUC+*, and transformants were identified via glufosinate ammonium resistance.

T3 and F3 seed were surface sterilized in chlorine gas and stratified in sterile water at 4°C for at least 3 days prior to plating on half-strength Murashige and Skoog (0.5 MS) medium (Prasetyaningrum et al., 2023). Seedlings were entrained for 5–12 d before being transferred to testing conditions as described in each figure legend. During standard growth, plants were kept under 150 μmol m^{-2} s^{-1} white light in 12 h:12 h light:dark cycles in Panasonic MLR-352-PE chambers. Relative humidity and temperature were set to 60%–70% and 22°C, respectively, except where growth under other temperatures conditions is listed.

Hypocotyl assays

Seeds were grown on 0.5 MS agar plates and irradiated with cool fluorescent white light at 170 μmol m^{-2} s^{-1} for 4 h before being moved to light chambers as per experimental requirements and grown vertically for 5 days before being imaged and processed using ImageJ (Schneider

et al., 2012). Short-day, long-day, and square-form treatments used 30 μmol m^{-2} s^{-1}, and the pseudo-sinusoidal light treatment used a cycle of 1 h 10 μmol m^{-2} s^{-1}, 8 h 40 μmol m^{-2} s^{-1}, 5 h 30 μmol m^{-2} s^{-1}, 4 h 10 μmol m^{-2} s^{-1}, and 6 h of darkness. Data were plotted and analyzed using a one-way ANOVA followed by Dunnett's multiple-comparisons test in GraphPad Prism v.10.0.3.

Luciferase assays

Individual seedlings were grown for 6 days in 12:12 light:dark cycles under white light on 0.5 MS medium as in previous work (Prasetyaningrum et al., 2023). Plants were sprayed with 3 mM D-luciferin in 0.1% Triton X-100 before being transferred to imaging conditions as described for each experiment. Individual plants were imaged repeatedly (every 1–2 h), dependent upon the experiment, using a Retiga LUMO camera run by MicroManager 1.4.23 (Edelstein et al., 2014) using a custom script. In experiments where temperature was not constant throughout growth and imaging, temperature change was initiated as indicated. The patterns of the luciferase signal were fitted to cosine waves using Fourier fast transform non-linear least squares (Plautz et al., 1997) to estimate the circadian period length made using BioDare2 (Zielinski et al., 2014) (www.biodare2.ed.ac.uk). Relative amplitude error (RAE) was calculated by dividing the amplitude error estimate for each curve by the amplitude value (Plautz et al., 1997). Data were considered rhythmic if the fitted curve returned a period estimate within 18–34 h and had an RAE < 0.6. Waveforms, periods, and percentage rhythmicity data were plotted using GraphPad Prism v.10.2.3.

RT–qPCR

Following entrainment, seedlings were transferred to constant darkness at dusk. Tissue was harvested and snap-frozen in liquid nitrogen at the indicated time points before RNA extraction using Tri Reagent according to the manufacturer's protocol (Sigma-Aldrich, Dorset, UK; http://www.sigmaaldrich.com). Reverse transcription was performed using either Superscript II or M-MLV reverse transcriptase according to the manufacturer's protocols (Invitrogen, Waltham, MA, USA; https://www.thermofisher.com/Invitrogen). Real-time reverse transcription polymerase chain reaction was performed using a QuantStudio 3 Real-Time PCR System or a StepOnePlus Real-Time PCR System (Applied Biosystems, Waltham, MA, USA; https://www.thermofisher.com/AppliedBiosystems). Samples were run in triplicate, and starting quantities were estimated from a critical threshold using the standard curve of amplification. *APA1*, *APX3*, and *IPP2* expression was used as an internal control, with data for each sample normalized to these as described previously (Nusinow et al., 2011).

RNA-seq

Plants were grown on 0.5 MS agar plates under entrainment conditions for 12 days. At dusk on the 12th day of growth (ZT12), seedlings were transferred to constant darkness. Pools of approximately 20 seedlings were harvested and snap frozen in liquid nitrogen 48 h later (ZT60). Total RNA was extracted from three biological replicates per genotype using Tri Reagent according to the manufacturer's protocol (Sigma-Aldrich). Library preparation and Illumina sequencing (Illumina, San Diego, CA, USA) with 150-bp paired-end reads was performed by Novogene Biotech (Cambridge, UK) using Illumina protocols. RNA-seq reads were first aligned to the AtRTD3 transcriptome (Zhang et al., 2022), and read counts were generated using Kallisto (Bray et al., 2016) in the Galaxy platform (Afgan et al., 2016). Subsequent analysis was performed using the 3DRNAseq pipeline (Guo et al., 2021). Transcript abundance was expressed as transcripts per million (TPM) for each gene product within each genotype. TPM values were used to calculate fold change difference in transcript accumulation relative to other genotypes. ANOVA was performed to compare the transcript abundance for a given transcript in each genotype to the other genotypes tested. This was followed by pairwise comparison via a post hoc Tukey test to determine the adjusted p values for each genotype pairing. Significant differential expression of a transcript was defined as two genotypes presenting a fold change difference of accumulation of log fold change (-log2FC) > 1 or -log2FC < −1 along with an adjusted $p < 0.05$. A list of transcripts contributing to circadian rhythmicity were derived from Hsu and Harmer (2014) and Laosuntisuk et al. (2023). GO annotation was performed using DAVID (Huang et al., 2009; Sherman et al., 2022). A list of 740 genes was taken from the GO term GO:0009416 "response to light stimulus" (Ashburner et al., 2000; Gene Ontology Consortium, 2023). Genes of interest were plotted in heatmaps and volcano plots using R (R Core Team, 2013) and RStudio (Posit Software).

Phase enrichment analysis was completed using CAST-R (Bonnot et al., 2022). Differentially accumulated transcripts for each genotype (Supplemental Table 1) were compared to the "Bonnot and Nagel Transcriptome LL" reference dataset. Data were summarized by presenting fold enrichment (i.e., the ratio between the proportion of the phase in the genotype-specific mis-regulated gene list and the proportion in the defined phase reference dataset (Bonnot et al., 2022). Statistical significance was determined using a chi-square test (Bonnot et al., 2022). Data were plotted using R (R Core Team, 2013) and RStudio (Posit Software).

Flowering time and growth analysis

Following stratification, plants were grown on soil until bolting. Rosette area, rosette diameter, and leaf counts were measured regularly throughout the growth period (approximately twice per week). The number of days to bolting were recorded when the bolt was 1 cm above the rosette. Plants were grown under 150 μmol m^{-2} s^{-1} white light with day length and temperature varied between experiments. For variable day length experiments, plants were grown under long days (16 h light:8 h darkness) or short days (8 h light:16 h darkness) at 22°C. For temperature response experiments, plants were grown under balanced day lengths (12 h light:12 h darkness) under either 27°C, 22°C, 17°C, or 12°C. Data were plotted and analyzed using a two-way ANOVA followed by Tukey's multiple comparisons test in GraphPad Prism v.10.2.3.

Ranking of phenotypic plasticity

Random regression mixed models were utilized to enable comparison of phenotypic plasticity between genotypes (Arnold et al., 2019). Akaike information criterion was used to evaluate model fit (Zuur et al., 2009). Optimal model fits for hypocotyl length and flowering time were achieved by fitting a quadratic fixed effects model for the fixed effect of growth temperature or photoperiod, with random effects allocated to genotype. Rosette diameter was best modeled by fitting a cubic fixed effects model for the fixed effect of growth temperature, with random effects allocated to genotype.

Mathematical modeling

FMv2 (Chew et al., 2022) is a multiscale model of *Arabidopsis* that brings together multiple modules to describe diverse processes, including the circadian clock, flowering, metabolism, and vegetative growth. The F2014 model (Fogelmark and Troein, 2014) is an updated *Arabidopsis* circadian clock model with fewer explicit light-sensitive reactions and without extended transcriptional activation. Both these models were used and combined in this study. The original FMv2 model was simulated, with minimal changes as described below to allow for introduction of the YHB mutant and for model comparison. The FMv2+F2014 model was constructed by replacing the P2011 (Pokhilko et al., 2012) circadian module of FMv2 with the updated F2014 circadian model, in the spirit of the modular framework model.

FMv2 model

The MATLAB code for the FMv2 was downloaded from the GitHub repository (https://github.com/danielseaton/frameworkmodel/;FAIRDOM link: https://fairdomhub.org/models/248) and run in MATLAB R2022a.

Addition of F2014

MATLAB code was written to simulate the F2014 model based on the equations described in Fogelmark and Troein (2014). ChatGPT4 was

initially used to convert the PDF image of the equations into LaTeX code. This was then manually corrected to remove errors introduced by the AI and then converted manually from LaTeX into MATLAB. Conversion to MATLAB was also performed using ChatGPT4, and the two were compared as an additional check.

The F2014 model replaced the P2011 module of the FMv2 model. Scaling factors were added to rescale the amplitudes of the outputs of the circadian module F2014 to match those of P2011 to allow input to the PIF-CONSTANS-FLOWERING LOCUS T (PIF-CO-FT; Seaton-Smith) module (Seaton et al., 2015). Furthermore, CCA1 and LHY are modeled separately in F2014, so the sum of the two was used to replace the LHY input to the PIF-CO-FT module; specifically:

$$LHY_{P2011} = \frac{LHY_{F2014}+CCA1_{F2014}}{1.561}$$

$$PRR7_{P2011} = \frac{PRR7_{F2014}}{2.6754}$$

$$Gln_{P2011} = 40.9 \cdot Gln_{F2014}$$

$$PRR5_{P2011} = 0.841 \cdot PRR5n_{F2014}$$

$$TOC1_{P2011} = 1.21 \cdot TOC1n_{F2014}$$

Parameter choice

The parameter set 1 of Fogelmark and Troein (2014) was used in all simulations of this model. Parameters as preset in FMv2 were used for all other modules, with the exception of parameters for the hypocotyl length calculation and the photothermal time threshold for flowering. These parameters were used unchanged for the mutant predictions.

Photothermal time threshold parameter for flowering

A single parameter value was used for both the FMv2 and the FMv2+F2014 models, which was fitted based on FMv2 using the laboratory's wild-type data for various photoperiods (Supplemental Figure 1B, bottom). The parameter value was 4107.6 modified photothermal units.

Hypocotyl length parameters

Hypocotyl length was calculated according to the equation used in Seaton et al. (2015):

$$Hyp_{length} = h_1 \int_0^{24} (z(t) - h_2)dt$$

where

$$z(t) = \begin{cases} c^{(m)}_{ATHB2}, if\ c^{(m)}_{ATHB2} < h_3 \\ h_3, if\ c^{(m)}_{ATHB2} \geq h_3 \end{cases}$$

Reparameterization was carried out for h_1, h_2, h_3 separately for each version of the model based on the data shown in Supplemental Figure 1B, top.

Parameter	FMv2	FMv2 + F2014
h_1	0.2657	0.3747
h_2	−0.3595	−0.1844
h_3	0.6158	0.7107

Simulating mutants

The *elf3* and YHB mutations were introduced in the P2011 and F2014 models. The *elf3* mutation is present in the original code for FMv2 (P2011), so this was simulated in the same way. For F2014, the ELF3 protein production parameter p_{16} was set to 0 in the mutant.

The YHB mutant was added in both circadian models, either "globally" by altering all light inputs except for blue light (assumed to affect the GI and ZTL protein light sensitivities and the dark accumulator) or by altering only COP1-related light inputs. The alteration in both cases was to set the relevant light input to be 75% ON in the dark (and 100% ON in the light as normal). This accounts for the activity of the constitutively active phyB signaling in the dark and phyB in combination with wild-type signaling from other photoreceptors and photosynthetically derived metabolites in the light. However, we note that this value of 75% is not interpreted as the biological contribution of YHB to clock signaling but is chosen to account for observed changes in flowering time while still producing robust circadian rhythms (Supplemental Figure 7).

YHB is also affecting the PIF-CO-FT module directly, where phyB is explicitly modeled. In this case, the light variable only for the phyB equation itself is set to 1 at all times in the mutant.

Model simulation

The ordinary differential equations were solved numerically using MATLAB's ode15s. The circadian module for both P2011 and F2014 was initialized and entrained for 12 days in 12:12 light:dark conditions prior to the simulation start. Initial conditions were set as in Chew et al. (2022) for P2011, while for F2014, the initial value 0.1 was used for all variables.

DATA AND CODE AVAILABILITY

Requests for further information, resources, and reagents should be directed to and will be fulfilled by M.A.J. (matt.jones@glasgow.ac.uk). Plasmids generated in this study are available upon request. RNA-seq data have been deposited at GEO and are publicly available (PRJNA1078346). Luciferase data have been deposited in BioDare2 (www.biodare2.ac.uk) with accession numbers 29131 (Figure 2A), 29135 (Figure 2E), 29136 (Figure 2G), 29133 (Figure 2J), and 29132 (Figure 4A). Any additional information required to re-analyze the data reported in this paper is available from the corresponding author upon request. Models of hypocotyl growth (Seaton et al., 2015) and flowering time (Chew et al., 2022) are derived from previously published work available at FAIRDOMHub (https://fairdomhub.org/models/248). All original code is publicly available at https://github.com/ReaAntKour/FMv2_F2014_model/releases/tag/v1.0.0.

SUPPLEMENTAL INFORMATION

Supplemental information is available at *Molecular Plant Online*.

FUNDING

This work was supported by the UKRI (BB/S005404/1 and BB/Z514469/1), the Gatsby Charitable Foundation, the Perry Foundation (to S.F.E.), the Douglas Bomford Trust (to S.F.E.), and a William H. Danforth Plant Sciences Fellowship (to K.N.E.).

AUTHOR CONTRIBUTIONS

Conceptualization, D.A.N. and M.A.J.; methodology, M.W.B., R.A.K., D.A.N., and M.A.J.; software, R.A.K.; validation, C.D., J.O., and M.W.B.; formal analysis, M.W.B., S.F.E., M.A.J., and J.O.; investigation, M.W.B., S.F.E., C.D., and J.O.; resources, C.D., K.N.E., R.B., and M.A.J.; data curation, M.W.B., S.F.E., C.D., and J.O.; writing – original draft, M.W.B. and

M.A.J.; visualization, M.W.B. and S.F.E.; supervision, D.A.N. and M.A.J.; project administration, D.A.N. and M.A.J.; funding acquisition, D.A.N. and M.A.J.

ACKNOWLEDGMENTS

The authors would like to thank Dr. Donald Reid (University of Glasgow) for advice on statistical analysis. The authors have applied for a patent in relation to this research (PCT/US33/70851).

Received: March 15, 2024
Revised: June 14, 2024
Accepted: July 11, 2024
Published: July 15, 2024

REFERENCES

Afgan, E., Baker, D., van den Beek, M., Blankenberg, D., Bouvier, D., Čech, M., Chilton, J., Clements, D., Coraor, N., Eberhard, C., et al. (2016). The Galaxy platform for accessible, reproducible and collaborative biomedical analyses: 2016 update. Nucleic Acids Res. **44**:W3–W10.

Arnold, P.A., Kruuk, L.E.B., and Nicotra, A.B. (2019). How to analyse plant phenotypic plasticity in response to a changing climate. New Phytol. **222**:1235–1241.

Ashburner, M., Ball, C.A., Blake, J.A., Botstein, D., Butler, H., Cherry, J.M., Davis, A.P., Dolinski, K., Dwight, S.S., Eppig, J.T., et al. (2000). Gene ontology: tool for the unification of biology. The Gene Ontology Consortium. Nat. Genet. **25**:25–29.

Balcerowicz, M., Mahjoub, M., Nguyen, D., Lan, H., Stoeckle, D., Conde, S., Jaeger, K.E., Wigge, P.A., and Ezer, D. (2021). An early-morning gene network controlled by phytochromes and cryptochromes regulates photomorphogenesis pathways in Arabidopsis. Mol. Plant **14**:983–996.

Bonnot, T., Gillard, M.B., and Nagel, D.H. (2022). CAST-R: An application to visualize circadian and heat stress-responsive genes in plants. Plant Physiol. **190**:994–1004.

Bray, N.L., Pimentel, H., Melsted, P., and Pachter, L. (2016). Near-optimal probabilistic RNA-seq quantification. Nat. Biotechnol. **34**:525–527.

Chen, F., Li, B., Li, G., Charron, J.-B., Dai, M., Shi, X., and Deng, X.W. (2014). Arabidopsis Phytochrome A Directly Targets Numerous Promoters for Individualized Modulation of Genes in a Wide Range of Pathways. Plant Cell **26**:1949–1966.

Chew, Y.H., Seaton, D.D., Mengin, V., Flis, A., Mugford, S.T., George, G.M., Moulin, M., Hume, A., Zeeman, S.C., Fitzpatrick, T.B., et al. (2022). The Arabidopsis Framework Model version 2 predicts the organism-level effects of circadian clock gene mis-regulation. silico Plants **4**:diac010.

Clough, S., and Bent, A. (1998). Floral dip: a simplified method for Agrobacterium-mediated transformation of *Arabidopsis thaliana*. Plant J. **16**:735–743.

Covington, M.F., Panda, S., Liu, X.L., Strayer, C.A., Wagner, D.R., and Kay, S.A. (2001). ELF3 modulates resetting of the circadian clock in Arabidopsis. Plant Cell **13**:1305–1315.

Edelstein, A.D., Tsuchida, M.A., Amodaj, N., Pinkard, H., Vale, R.D., and Stuurman, N. (2014). Advanced methods of microscope control using μManager software. J. Biol. Methods **1**:e10.

Ezer, D., Jung, J.H., Lan, H., Biswas, S., Gregoire, L., Box, M.S., Charoensawan, V., Cortijo, S., Lai, X., Stöckle, D., et al. (2017). The evening complex coordinates environmental and endogenous signals in Arabidopsis. Nat. Plants **3**:17087.

Fehér, B., Kozma-Bognár, L., Kevei, E., et al. (2011). Functional interaction of the circadian clock and UV RESISTANCE LOCUS 8-controlled UV-B signaling pathways in *Arabidopsis thaliana*. Plant J. **67**:37–48.

Fogelmark, K., and Troein, C. (2014). Rethinking Transcriptional Activation in the Arabidopsis Circadian Clock. PLoS Comput. Biol. **10**:e1003705.

Franklin, K.A., and Quail, P.H. (2010). Phytochrome functions in Arabidopsis development. J. Exp. Bot. **61**:11–24.

Gene Ontology Consortium, Aleksander, S.A., Balhoff, J., Carbon, S., Cherry, J.M., Drabkin, H.J., Ebert, D., Feuermann, M., Gaudet, P., Harris, N.L., et al. (2023). The Gene Ontology knowledgebase in 2023. Genetics **224**:iyad031.

Graf, A., Schlereth, A., Stitt, M., and Smith, A.M. (2010). Circadian control of carbohydrate availability for growth in Arabidopsis plants at night. Proc. Natl. Acad. Sci. USA **107**:9458–9463.

Guo, W., Tzioutziou, N.A., Stephen, G., Milne, I., Calixto, C.P., Waugh, R., Brown, J.W.S., and Zhang, R. (2021). 3D RNA-seq: a powerful and flexible tool for rapid and accurate differential expression and alternative splicing analysis of RNA-seq data for biologists. RNA Biol. **18**:1574–1587.

Hajdu, A., Adam, E., Sheerin, D.J., Dobos, O., Bernula, P., Hiltbrunner, A., Kozma-Bogn√°r, L., and Nagy, F. (2015). High-level expression and phosphorylation of phytochrome B modulates flowering time in Arabidopsis. Plant J. **83**:794–805.

Haydon, M.J., Mielczarek, O., Robertson, F.C., Hubbard, K.E., and Webb, A.A.R. (2013). Photosynthetic entrainment of the *Arabidopsis thaliana* circadian clock. Nature **502**:689–692.

Hicks, K.A., Millar, A.J., Carré, I.A., Somers, D.E., Straume, M., Meeks-Wagner, D.R., and Kay, S.A. (1996). Conditional Circadian Dysfunction of the Arabidopsis early-flowering 3 Mutant. Science (New York, NY) **274**:790–792.

Hsu, P.Y., and Harmer, S.L. (2014). Wheels within wheels: The plant circadian system. Trends Plant Sci. **19**:240–249.

Hu, W., Figueroa Balderas, R., Chi Ham, C., and Lagarias, J.C. (2020). Regulation of monocot and dicot plant development with constitutively active alleles of phytochrome B. Plant Direct **4**:401.

Hu, W., Su, Y.-S., and Lagarias, J.C. (2009). A light-independent allele of phytochrome B faithfully recapitulates photomorphogenic transcriptional networks. Mol. Plant **2**:166–182.

Huang, D.W., Sherman, B.T., and Lempicki, R.A. (2009). Systematic and integrative analysis of large gene lists using DAVID bioinformatics resources. Nat. Protoc. **4**:44–57.

Huang, H., Alvarez, S., Bindbeutel, R., Shen, Z., Naldrett, M.J., Evans, B.S., Briggs, S.P., Hicks, L.M., Kay, S.A., and Nusinow, D.A. (2016a). Identification of Evening Complex Associated Proteins in Arabidopsis by Affinity Purification and Mass Spectrometry. Mol. Cell. Proteomics **15**:201–217.

Huang, H., Gehan, M.A., Huss, S.E., Alvarez, S., Lizarraga, C., Gruebbling, E.L., Gierer, J., Naldrett, M.J., Bindbeutel, R.K., Evans, B.S., et al. (2017). Cross-species complementation reveals conserved functions for EARLY FLOWERING 3 between monocots and dicots. Plant Direct **1**:e00018.

Huang, H., McLoughlin, K.E., Sorkin, M.L., Burgie, E.S., Bindbeutel, R.K., Vierstra, R.D., and Nusinow, D.A. (2019). PCH1 regulates light, temperature, and circadian signaling as a structural component of phytochrome B-photobodies in Arabidopsis. Proc. Natl. Acad. Sci. USA **116**:8603–8608.

Huang, H., Yoo, C.Y., Bindbeutel, R., Goldsworthy, J., Tielking, A., Alvarez, S., Naldrett, M.J., Evans, B.S., Chen, M., and Nusinow, D.A. (2016b). PCH1 integrates circadian and light-signaling pathways to control photoperiod-responsive growth in Arabidopsis. Elife **5**:e13292.

Jiang, Y., Yang, C., Huang, S., Xie, F., Xu, Y., Liu, C., and Li, L. (2019). The ELF3-PIF7 interaction mediates the circadian gating of the shade response in Arabidopsis. iScience **22**:288–298.

Jones, M.A., Hu, W., Litthauer, S., Lagarias, J.C., and Harmer, S.L. (2015). A Constitutively Active Allele of Phytochrome B Maintains Circadian Robustness in the Absence of Light. Plant Physiol. **169**:814–825.

Jones, M.A. (2018). Interplay of circadian rhythms and light in the regulation of photosynthesis-derived metabolism. Prog. Bot. **79**:147–171.

Jones, M.A. (2019). Retrograde signalling as an informant of circadian timing. New Phytol. **221**:1749–1753.

Jung, J.-H., Domijan, M., Klose, C., Biswas, S., Ezer, D., Gao, M., Khattak, A.K., Box, M.S., Charoensawan, V., Cortijo, S., et al. (2016). Phytochromes function as thermosensors in Arabidopsis. Science **354**:886–889.

Jung, J.H., Barbosa, A.D., Hutin, S., Kumita, J.R., Gao, M., Derwort, D., Silva, C.S., Lai, X., Pierre, E., Geng, F., et al. (2020). A prion-like domain in ELF3 functions as a thermosensor in Arabidopsis. Nature **585**:256–260.

Kerbler, S.M., and Wigge, P.A. (2023). Temperature Sensing in Plants. Annu. Rev. Plant Biol. **74**:341–366.

Kim, J., Geng, R., Gallenstein, R.A., and Somers, D.E. (2013). The F-box protein ZEITLUPE controls stability and nucleocytoplasmic partitioning of GIGANTEA. Development **140**:4060–4069.

Kolmos, E., Herrero, E., Bujdoso, N., Millar, A.J., T√≥th, R., Gyula, P., Nagy, F., and Davis, S.J. (2011). A reduced-function allele reveals that EARLY FLOWERING3 repressive action on the circadian clock is modulated by phytochrome signals in Arabidopsis. Plant Cell **23**:3230–3246.

Koushik, S.V., Chen, H., Thaler, C., Puhl, H.L., and Vogel, S.S. (2006). Cerulean, Venus, and VenusY67C FRET reference standards. Biophys. J. **91**:L99–L101.

Laosuntisuk, K., Elorriaga, E., and Doherty, C.J. (2023). The Game of Timing: Circadian Rhythms Intersect with Changing Environments. Annu. Rev. Plant Biol. **74**:511–538.

Legris, M., Klose, C., Burgie, E.S., Rojas, C.C.R., Neme, M., Hiltbrunner, A., Wigge, P.A., Schäfer, E., Vierstra, R.D., and Casal, J.J. (2016). Phytochrome B integrates light and temperature signals in Arabidopsis. Science **354**:897–900.

Liu, X.L., Covington, M.F., Fankhauser, C., Chory, J., and Wagner, D.R. (2001). ELF3 encodes a circadian clock-regulated nuclear protein that functions in an Arabidopsis PHYB signal transduction pathway. Plant Cell **13**:1293–1304.

McWatters, H., Bastow, R., Hall, A., and Millar, A. (2000). The ELF3 zeitnehmer regulates light signalling to the circadian clock. Nature **408**:716–720.

Millar, A.J. (2016). The Intracellular Dynamics of Circadian Clocks Reach for the Light of Ecology and Evolution. Annu. Rev. Plant Biol. **67**:595–618.

Nieto, C., Catalán, P., Luengo, L.M., Legris, M., López-Salmerón, V., Davière, J.M., Casal, J.J., Ares, S., and Prat, S. (2022). COP1 dynamics integrate conflicting seasonal light and thermal cues in the control of Arabidopsis elongation. Sci. Adv. **8**:eabp8412.

Nusinow, D.A., Helfer, A., Hamilton, E.E., King, J.J., Imaizumi, T., Schultz, T.F., Farr√©, E.M., and Kay, S.A. (2011). The ELF4-ELF3-LUX complex links the circadian clock to diurnal control of hypocotyl growth. Nature **475**:398–402.

Plautz, J.D., Straume, M., Stanewsky, R., Jamison, C.F., Brandes, C., Dowse, H.B., Hall, J.C., and Kay, S.A. (1997). Quantitative analysis of Drosophila period gene transcription in living animals. J. Biol. Rhythms **12**:204–217.

Pokhilko, A., Fernandez, A.P., Edwards, K.D., Southern, M.M., Halliday, K.J., and Millar, A.J. (2012). The clock gene circuit in Arabidopsis includes a repressilator with additional feedback loops. Mol. Syst. Biol. **8**:574.

Prasetyaningrum, P., Litthauer, S., Vegliani, F., Battle, M.W., Wood, M.W., Liu, X., Dickson, C., and Jones, M.A. (2023). Inhibition of RNA degradation integrates the metabolic signals induced by osmotic stress into the Arabidopsis circadian system. J. Exp. Bot. **74**:5805–5819.

Queiroz, M.V., Battle, M.W., and Jones, M.A. (2023). Interactions between photosynthesis and the circadian system. Understanding and improving crop photosynthesis: Burleigh Dodds Series in Agricultural Science, 75–92.

R Core Team. (2013). R: A Language and Environment for Statistical Computing.

Reed, J.W., Nagpal, P., Bastow, R.M., Solomon, K.S., Dowson-Day, M.J., Elumalai, R.P., and Millar, A.J. (2000). Independent action of ELF3 and phyB to control hypocotyl elongation and flowering time. Plant Physiol. **122**:1149–1160.

Sanchez, S.E., Rugnone, M.L., and Kay, S.A. (2020). Light Perception: A Matter of Time. Mol. Plant **13**:363–385.

Schneider, C.A., Rasband, W.S., and Eliceiri, K.W. (2012). NIH Image to ImageJ: 25 years of image analysis. Nat. Methods **9**:671–675.

Seaton, D.D., Smith, R.W., Song, Y.H., MacGregor, D.R., Stewart, K., Steel, G., Foreman, J., Penfield, S., Imaizumi, T., Millar, A.J., et al. (2015). Linked circadian outputs control elongation growth and flowering in response to photoperiod and temperature. Mol. Syst. Biol. **11**:776.

Sherman, B.T., Hao, M., Qiu, J., Jiao, X., Baseler, M.W., Lane, H.C., Imamichi, T., and Chang, W. (2022). DAVID: a web server for functional enrichment analysis and functional annotation of gene lists (2021 update). Nucleic Acids Res. **50**:W216–W221.

Somers, D.E., Kim, W.Y., and Geng, R. (2004). The F-box protein ZEITLUPE confers dosage-dependent control on the circadian clock, photomorphogenesis, and flowering time. Plant Cell **16**:769–782.

Somers, D.E., Devlin, P.F., and Kay, S.A. (1998). Phytochromes and cryptochromes in the entrainment of the Arabidopsis circadian clock. Science **282**:1488–1490.

Sorin, C., Salla-Martret, M., Bou-Torrent, J., Roig-Villanova, I., and Martínez-García, J.F. (2009). ATHB4, a regulator of shade avoidance, modulates hormone response in Arabidopsis seedlings. Plant J. **59**:266–277.

Su, Y.S., and Lagarias, J.C. (2007). Light-independent phytochrome signaling mediated by dominant GAF domain tyrosine mutants of Arabidopsis phytochromes in transgenic plants. Plant Cell **19**:2124–2139.

Thines, B., and Harmon, F.G. (2010). Ambient temperature response establishes ELF3 as a required component of the core Arabidopsis circadian clock. Proc. Natl. Acad. Sci. USA **107**:3257–3262.

Ushijima, T., Hanada, K., Gotoh, E., Yamori, W., Kodama, Y., Tanaka, H., Kusano, M., Fukushima, A., Tokizawa, M., Yamamoto, Y.Y., et al. (2017). Light Controls Protein Localization through Phytochrome-Mediated Alternative Promoter Selection. Cell **171**:1316–1325.e12.

Wagner, D., Tepperman, J.M., and Quail, P.H. (1991). Overexpression of phytochrome B induces a short hypocotyl phenotype in transgenic Arabidopsis. Plant Cell **3**:1275–1288.

Wang, Q., Liu, W., Leung, C.C., Tarté, D.A., and Gendron, J.M. (2024). Plants distinguish different photoperiods to independently control seasonal flowering and growth. Science **383**:eadg9196.

Webb, A.A.R., Seki, M., Satake, A., and Caldana, C. (2019). Continuous dynamic adjustment of the plant circadian oscillator. Nat. Commun. **10**:550.

Yu, J.-W., Rubio, V., Lee, N.Y., Bai, S., Lee, S.Y., Kim, S.S., Liu, L., Zhang, Y., Irigoyen, M.L., Sullivan, J.A., et al. (2008). COP1 and ELF3 Control Circadian Function and Photoperiodic Flowering by Regulating GI Stability. Mol. Cell **32**:617–630.

Zagotta, M.T., Hicks, K.A., Jacobs, C.I., Young, J.C., Hangarter, R.P., and Meeks-Wagner, D.R. (1996). The Arabidopsis ELF3 gene regulates vegetative photomorphogenesis and the photoperiodic induction of flowering. Plant J. **10**:691–702.

Zhang, R., Kuo, R., Coulter, M., Calixto, C.P.G., Entizne, J.C., Guo, W., Marquez, Y., Milne, L., Riegler, S., Matsui, A., et al. (2022). A high-resolution single-molecule sequencing-based Arabidopsis transcriptome using novel methods of Iso-seq analysis. Genome Biol. **23**:149.

Zielinski, T., Moore, A.M., Troup, E., Halliday, K.J., and Millar, A.J. (2014). Strengths and limitations of period estimation methods for circadian data. PLoS One **9**:e96462.

Zuur, A.F., Ieno, E.N., Walker, N.J., Saveliev, A.A., and Smith, G.M. (2009). Mixed Effects Models and Extensions in Ecology with R (Springer), p. 574.